Analytic three-channel model for resonance-averaged direct and indirect dissociative recombination processes of molecular ions

I. F. Schneider,[1] N. Pop,[2] and Ch. Jungen[3]

[1]*Laboratoire Ondes et Milieux Complexes, UMR-6294 CNRS et Université du Havre, 25, rue Philippe Lebon, BP 540, 76058 Le Havre, France*

[2]*Department of Physical Foundations of Engineering, Polytechnical University of Timisoara, RO-300223 Timisoara, Romania*

[3]*Laboratoire Aimé Cotton du CNRS, Bâtiment 505, Université de Paris-Sud, F-91405 Orsay, France*

(Received 3 October 2012; published 17 December 2012)

An analytic three-channel model is developed for the description of simultaneous direct and indirect dissociative recombination (DR) cross sections of molecular ions with electrons. The model is formulated in terms of three parameters describing the interactions between the electron-ion entrance channel e, the dissociation channel d, and an "active" quasibound molecular Rydberg channel a and yields resonance-averaged cross sections for low incident electron energies. The relative magnitudes of the parameters determine (i) the height of the downward steps at the ion vibrational thresholds and (ii) the relative contributions of the direct and indirect processes. The model is intended to serve for the empirical analysis of observed DR cross sections, and in particular it allows the assessment of the extent to which reionization of the capture complex competes with dissociation. The model is applied to the DR of H_3^+ and HCO^+.

DOI: 10.1103/PhysRevA.86.062706 PACS number(s): 34.10.+x, 34.80.Lx, 33.20.Wr

I. INTRODUCTION

The dissociative recombination of molecular ions with electrons is an important process in interstellar medium and plasmas. Bates [1] originally envisioned this process as being due to a *direct* coupling between the ionization (entrance) channel and the dissociation (exit) channel. In his theory these are represented by potential energy curves pertaining to the relevant nuclear reaction coordinate, namely, the electronic potential energy curve of the ion for the entrance channel and the potential curve describing the dissociating neutral particles in the exit channel. The DR process is favored when the dissociative curve crosses the ion curve near its minimum. It was many years after Bates's seminal work when Bardsley [2] (see also Ref. [3]) recognized that in some systems no such favorable crossing occurs, but the DR process still proceeds via an *indirect* two-step mechanism. The indirect process involves resonant capture of the colliding electron in a quasibound Rydberg series of the neutral species, followed by predissociation into neutral fragments.

Indirect processes are characterized by conspicuous *downward steps* or "kinks" of the DR cross section near the convergence threshold of the active quasibound Rydberg series [6,7]. Such kinks turn out to be rather widespread in many larger systems including even small molecular clusters [7], to the extent that one may wonder whether the original assumption should be revised, according to which the prevalence of a direct process would be the "normal" situation, whereas the indirect process is exceptional. The kinks stand out in experimental cross-sectional plots and appear conspicuously as steps because in most cases the experimental energy resolution has not been sufficient to resolve the Rydberg structure of the vibrationally excited capture states. To date H_2^+ and H_3^+ are the only exceptions where it has been possible to resolve a few of these resonances experimentally.

Previous theoretical treatments of indirect processes in polyatomic systems [4–8] therefore focused on the DR cross section, $\langle\sigma\rangle$, averaged over the Rydberg resonances. This simplified approach was based on the Breit-Wigner (BW) formula, and it was assumed that once the electron is captured the compound molecule immediately dissociates and there is no possibility for it to reionize by re-ejecting the electron into the electronic (ionization) continuum. Thus the capture process is the rate-determining step and is the only one that needs to be considered explicitly. Further it was assumed that above the vibrational threshold where the active Rydberg series has terminated, the capture probability and therefore also DR cross section σ drop to zero. Both these assumptions correspond to extreme situations and are not exactly verified in real quantum systems.

The physical reasons for the kinks to appear are twofold. First, the incoming electron is likely to be re-ejected into the newly opened ionization channel and dissociation is therefore decreased. Second, despite the presence of Rydberg series associated with higher vibrational thresholds, these are in fact not directly coupled to the electronic continuum associated with the ground-level ion and therefore cannot efficiently capture the electron. (We have verified this point with numerical multichannel scattering calculations in which the $\Delta v = 2$ coupling was arbitrarily set to zero or alternatively to a large value, while the $\Delta v = 1$ couplings were kept fixed at a large value. The kink was present in the first case but disappeared in the second situation.) The coupling is weak since now the ion core has to take up two (or more) quanta of vibrational energy, a process which is essentially forbidden owing to the $\Delta v = 1$ propensity rule [9,10]. The propensity rule states that in electron-vibrating-ion collisions the nonadiabatic energy exchange between the continuum electron and the vibrating ion essentially proceeds via the route involving the smallest possible change of the vibrational quantum number v of the ion, with the $\Delta v = 1$ process very strongly favored when energetically possible. The validity of this propensity rule has been verified in great detail experimentally and theoretically in the Rydberg states of H_2 [10,11] and many other systems [12].

The analytic expressions for the resonance-averaged DR cross section used in Refs. [5–7] read

$$\langle\sigma\rangle = \frac{4\pi r}{k^2}(\pi\mu_{ea})^2, \quad \epsilon = \frac{1}{2}k^2 \leqslant E_a^+,$$
$$\sigma = 0, \quad \epsilon = \frac{1}{2}k^2 > E_a^+. \tag{1}$$

Here k is the wave number of the incident electron in inverse bohr units, a_0^{-1}, r is the multiplicity ratio which implies averaging over the degeneracy of the initial electron + target ion state and summing over the degeneracy of the final molecular state, ϵ is the energy of the incident electron in atomic units [i.e., $\epsilon = E/(\hbar^2/ma_0^2)$, where m is the electron mass and E is in SI units], E_a^+ is the convergence threshold of the active Rydberg channel, and μ_{ea} is a dimensionless quantum defect matrix element connecting the continuum entrance channel e to the active Rydberg channel a. $\pi\mu_{ea}$ is the associated electron-ion phase shift matrix element relevant for the capture process. In Refs. [6,7] it proved possible to derive the quantum defect μ_{ea} from bound-state Rydberg spectroscopic information, using the fact that quantum defects typically vary slowly with energy and thus have very nearly the same values below and above the threshold.

Figure 1 illustrates the application of Eq. (1) to the dissociative recombination of H_3^+ [6] (dot-dashed and full curves, green online). The kink at the $v_2^+ = 1$ threshold is clearly exhibited by the experimental data, and, as pointed out in Ref. [13], a second smaller step appears also at the $v_2^+ = 2$ threshold. Equation (1), implemented with the parameter μ_{ea} deduced from bound-state Rydberg spectroscopy [6,13], is seen to reproduce the observed [14,15] rate coefficient (cross section times electron velocity) quite well, in particular when

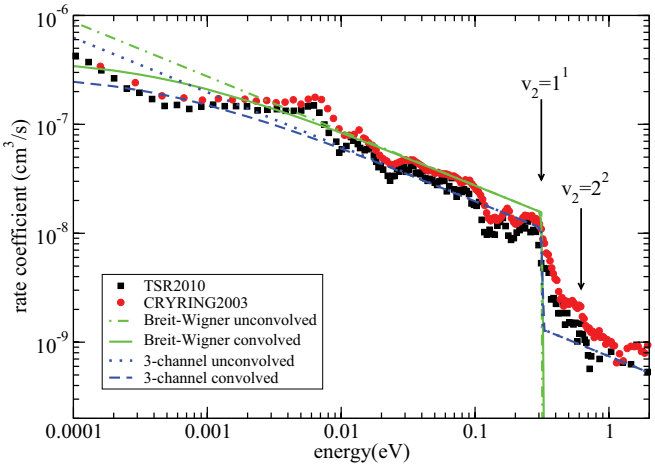

FIG. 1. (Color online) e^--H_3^+ dissociative recombination rate coefficients. Squares (black) and circles (red online): TSR (Ref. [14]) and CRYRING (Ref. [15]) experiments. Dot-dashed curve (green online): Eq. (1) (after Ref. [6]) unconvolved; full curve (green online): Eq. (1) convolved with $\Delta E_\perp = 1$ meV, $\Delta E_\parallel = 0.04$ meV. Dotted line (blue online): three-channel model [Eq. (20)] unconvolved; dashed line (blue online): three-channel model convolved. Note that the previous all-degrees-of-freedom computations of dos Santos *et al.* [16] and Petrignani *et al.* [17] (not shown here for clarity) produce excellent agreement throughout the energy range shown, including some of the resonance structure.

the spread of electron energies present in the experiments is taken into account (full curve, green online). The agreement demonstrates that the DR process in H_3^+ is essentially a $\Delta v_2^+ = 1$ process, governed by the propensity rule mentioned above. However, Eq. (1) does not reproduce the finite step height seen at the $v_2^+ = 1$ threshold because the Breit-Wigner theory does not account for the continuum-continuum interactions between the channels e and a above E_a^+. It is important to note that the all-degrees-of-freedom computations of dos Santos *et al.* [16] and Petrignani *et al.* [17] (not shown here for clarity) achieve excellent agreement with experiment both below and above the $v_2^+ = 1$ threshold, including some of the resonance structure.

In this paper we develop a three-channel analytical model for Rydberg averaged DR cross sections where these extreme conditions are relaxed and where in addition the possibility is provided for indirect and direct processes to be present simultaneously. The development is intended, first of all, as a test of the Breit-Wigner formula, Eq. (1). It should also be of use as an empirical tool for the interpretation of observed DR cross sections in situations where a full many-channel *ab initio* treatment of DR has not yet been implemented or is not possible at all at this time. We use Eq. (1) as a reference expression with which the more refined expressions derived below are compared.

II. THEORETICAL CONSIDERATIONS

A. Theoretical model

Figure 2 depicts the model channel structure which we are considering here. The entrance channel e is defined by the recombining ion in the vibrational state v_e^+ (typically $v_e^+ = 0$ in a cold environment like the interstellar medium) and the incoming electron electron with energy ϵ and wave number k in a given partial wave. The exit channel d corresponds to the dissociating fragments A and B, which may be atoms or neutral molecules. The active Rydberg channel a corresponds to an excited ion state, typically $v_a^+ = 1$, and represents the entrance channel for an indirect process in the sense that its coupling to e is favored by the $\Delta v^+ = 1$ rule. In our discussion channels e and d are open by definition, whereas the active Rydberg channel a may be closed (energy range below E_a^+) or open (energy range above E_a^+, cf. Fig. 2). In the following we call an "indirect" process one which proceeds via the intermediate Rydberg channel a whether or not the latter is closed. This corresponds to the spirit of multichannel quantum defect theory, which aims at treating open and closed channels on the same footing. Bardsley, in his work on indirect processes [2], considered only the bound portion of the active Rydberg series.

The channel structure represented in Fig. 2 is generic as it includes the minimal number of channels required to formally describe simultaneous direct and indirect DR processes. In a real molecule, of course, further Rydberg channels also exist which are associated with higher vibrational thresholds $v_a^+ = 2, 3, \ldots$. These may produce Rydberg structures in the energy region of interest here and may, for example, via a sequence of $\Delta v^+ = 1$ interactions, mediate the transition to the exit channel d. In a large polyatomic molecule there

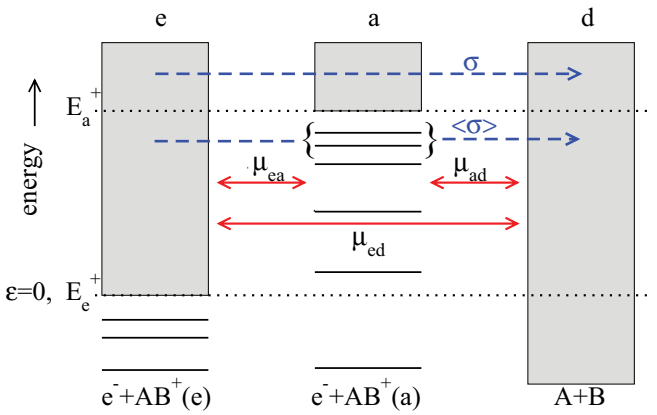

FIG. 2. (Color online) Three-channel model for dissociative recombination in a molecule, including an entrance-electron–molecular-ion channel e, a dissociation channel corresponding to fragmentation into neutral atomic and/or molecular fragments d, and an "active" quasibound Rydberg channel a (schematic). Continua are indicated by hatching, while bound levels are represented by horizontal bars. The two ion thresholds $E_e{}^+$ and $E_a{}^+$ correspond to ions in the vibrational ground and first excited states, respectively. The incident electron energy is zero ($\epsilon = 0$) for $E = E_e{}^+$. μ_{ij} ($i,j = e,a$, and d) are quantum defect matrix elements connecting the channels (double arrows, red online). $\zeta_{ij} = \tan \pi \mu_{ij}$ are the related reaction matrix elements. The channel couplings are assumed to be the same throughout the energy range shown. Dashed arrows (blue online) denoted by $\langle\sigma\rangle$ and σ refer, respectively, to the resonance-averaged DR cross section below and the continuum cross section above the threshold $E_a{}^+$.

may be an analogy with the phenomenon of intramolecular vibrational redistribution (IVR) (see, e.g., Ref. [18]), in that once the electron is captured, the system rapidly passes into the large manifold of vibrational degrees of freedom, before it eventually finds the way to the exit channel. The effect of these multistep interactions is lumped together in the effective coupling μ_{ad} (cf. the figure), which is directly related to the predissociation partial widths Γ_d of the a Rydberg resonances. Similarly, the coupling μ_{ea} is related to the autoionization partial widths Γ_e of the resonances [cf. the figure and Eq. (25)]. These considerations indicate that the effective three-channel scenario depicted in Fig. 2 is a reasonable starting point for an analytical model.

B. Basic expressions

The DR cross section is expressed in terms of the relevant scattering matrix element as

$$\sigma_{ed} = \frac{\pi r}{k^2} |S_{ed}|^2, \tag{2}$$

where, as above, k is the wave number of the incident electron.

Our task here is to evaluate S_{ed} in terms of the channel couplings between the three channels. Following Seaton [19], these latter may be expressed in terms of a quantum defect matrix $\boldsymbol{\mu}$ or in terms of the equivalent real reaction matrix $\mathbf{K} = \tan \pi\ \boldsymbol{\mu}$. The reaction matrix may be redefined in terms of cos- and sin-type matrices instead of tan, according to $\mathbf{K} = \mathcal{S}\mathcal{C}^{-1}$. These define the so-called complex Jost matrices,

$$\mathbf{J}^+ = \mathcal{C} + i\mathcal{S}, \quad \mathbf{J}^- = \mathcal{C} - i\mathcal{S}, \tag{3}$$

which in turn yield the generalized scattering matrix $\mathbf{X}$

$$\mathbf{X} = \mathbf{J}^+(\mathbf{J}^-)^{-1}. \tag{4}$$

The generalized scattering matrix may contain closed, c, as well as open, o, channels; that is, it has a block structure:

$$\mathbf{X} = \begin{pmatrix} \mathbf{X}_{oo} & \mathbf{X}_{oc} \\ \mathbf{X}_{co} & \mathbf{X}_{cc} \end{pmatrix}. \tag{5}$$

Finally, the physical scattering matrix is obtained after application of asymptotic boundary conditions to the closed channels, requiring that the closed-channel components of the wave function vanish at infinity. This is done by standard procedures [19] and yields

$$\mathbf{S} = \mathbf{X}_{oo} - \mathbf{X}_{oc} \frac{1}{\mathbf{X}_{cc} - e^{-2i\pi\nu}} \mathbf{X}_{co}. \tag{6}$$

Here $\boldsymbol{\nu}$ is in general a diagonal matrix consisting of the effective principal quantum numbers of all closed channels. In the present case only the active Rydberg channel may be closed (energy region lower than $E_a{}^+$), and we have the single value $\nu_a = [(E_a^+ - E)/\mathcal{R}hc]^{-1/2}$ where $\mathcal{R}$ is the Rydberg constant. The oscillating term $e^{-2i\pi\nu}$ in Eq. (6) produces an infinite number of resonances in the scattering matrix, which represent an infinite series of quasibound Rydberg states embedded in the continua. In this work we focus on the DR cross section *averaged* over the resonances. According to Gailitis [19,21] one has, instead of Eq. (6), in our three-channel situation with a single closed channel (energy range $E_e{}^+ \leqslant E \leqslant E_a{}^+$ in Fig. 2),

$$\langle |S_{ed}|^2 \rangle = |X_{ed}|^2 + \frac{|X_{ea}|^2 |X_{ad}|^2}{|X_{ea}|^2 + |X_{ad}|^2}. \tag{7}$$

For energies $E \geqslant E_a{}^+$ the second term of Eq. (7) is absent and one uses directly the appropriate element $|S_{ed}|^2 = |X_{ed}|^2$ in the cross section expression (2).

C. Construction of the generalized scattering matrix

The $\mathbf{X}$ matrix connecting ionization and dissociation channels required to implement Eqs. (2) and (7) may be constructed fully in a single step [16,22,23]. Alternatively it may be set up by means of techniques pioneered by Giusti [24], in two (or more) steps, by successively adding the interactions between the relevant channels. We use here this latter technique, which is particularly well adapted to indirect DR processes in polyatomic molecules mediated by vibronic Renner-Teller (RT) and Jahn-Teller (JT) interactions. Such interactions are exactly zero for certain nuclear geometries—for instance the linear configuration in HCO or the equilateral triangular configuration in H_3—and are therefore naturally introduced in a separate step. Giusti's two-step approach has been widely used for the description of direct processes mediated by electronic Rydberg-valence state interactions (configuration interaction). A recent example is afforded by the work of Waffeu Tamo *et al.* on the DR of HD^+ [25].

In the two-step approach one starts out from a zero-order generalized reaction matrix $\mathbf{K}^{(1)}$ to which one adds a further reaction matrix $\mathbf{K}^{(2)}$ arising from a residual interaction (e.g., the dissociative Rydberg-valence coupling or the RT or JT effects induced by distortion of the molecule). The total reaction matrix $\mathbf{K}^{(\text{total})}$ is not simply the sum; in other words, $\mathbf{K}^{(\text{total})} \neq \mathbf{K}^{(1)} + \mathbf{K}^{(2)}$. Instead, $\mathbf{K}^{(1)}$ and $\mathbf{K}^{(2)}$ must be combined by use of the eigenvector matrices of $\mathbf{K}^{(1)}$ and $\mathbf{K}^{(2)}$, with elements $U^{(1)}_{i\gamma}$ and $U^{(2)}_{\gamma\alpha}$, respectively, and eigenvalues $\tan\pi\mu_\gamma$ and $\tan\pi\mu_\alpha$. Eigenchannel Jost-type matrices analogous to Eq. (3) are then defined with elements $J_{i\alpha}{}^{\pm} = U_{i\alpha}e^{\pm i\pi\mu_\alpha}$, and the elements of the scattering matrix $\mathbf{X}^{(\text{total})}$ become [26]

$$X^{(\text{total})}_{ii'} = \sum_{\gamma\gamma'} U^{(1)}_{i\gamma} e^{i\pi\mu_\gamma} \left[\sum_{\alpha} U^{(2)}_{\gamma\alpha} e^{2i\pi\mu_\alpha} U^{(2)tr}_{\alpha\gamma'} \right] e^{i\pi\mu_{\gamma'}} U^{(1)tr}_{\gamma' i'}. \tag{8}$$

Note that when the zeroth-order reaction matrix $\mathbf{K}^{(1)}$ is diagonal, one has $U_{i\gamma} = \delta_{i\gamma}$ and the sums over γ and γ' in Eq. (8) may be dropped. The off-diagonal element $X^{(\text{total})}_{ed}$ which is of interest here is then independent of the zeroth-order quantum defects μ_γ. In what follows μ_{ij} refers to (real) quantum defect matrix elements in all cases, while $\mu_{\alpha \text{ or } \gamma}$ refers to eigen-quantum defects. We designate the real reaction matrix elements pertaining to one particular step by lowercase symbols $\zeta_{ij} \equiv \tan\pi\mu_{ij}$ in order to distinguish them from their counterparts in the total reaction matrix, $\mathbf{K}^{(\text{total})}$. Similarly, symbols ξ are used to denote complex matrix elements of a Jost matrix pertaining to one particular step of the treatment.

D. General structure of the two-step, three-channel problem

We define the reaction matrix (first step) connecting the asymptotic channels e, a, and d in such a way that only coupling between the Rydberg channels e and a is included and coupling with the dissociation channel d is ignored:

$$K^{(1)}_{ii'} = \begin{array}{c} \\ e \\ a \\ d \end{array} \begin{array}{c} \begin{array}{ccc} e & a & d \end{array} \\ \begin{pmatrix} \zeta_{ee} & \zeta_{ea} & 0 \\ \zeta_{ae} & \zeta_{aa} & 0 \\ 0 & 0 & 0 \end{pmatrix} \end{array}. \tag{9}$$

As already stated the elements ζ_{ij} are real. According to Eq. (8) the corresponding Jost matrices have the formal structure

$$\mathbf{J}^{(1)}_{i\gamma} = U^{(1)}_{i\gamma} e^{i\pi\mu_\gamma} = \begin{array}{c} \\ e \\ a \\ d \end{array} \begin{array}{c} \begin{array}{ccc} \gamma = 1 & 2 & 3 \end{array} \\ \begin{pmatrix} \cos\delta\, e^{i\pi\tau_1} & \sin\delta\, e^{i\pi\tau_2} & 0 \\ -\sin\delta\, e^{i\pi\tau_1} & \cos\delta\, e^{i\pi\tau_2} & 0 \\ 0 & 0 & 1 \end{pmatrix} \end{array}. \tag{10}$$

Here δ is a phase angle which accounts for the interaction between e and a, and $\pi\tau_1$, $\pi\tau_2$, and $\pi\tau_3 = 0$ are the corresponding eigenphases $\pi\mu_\gamma$ defined by $\tan\pi\mu_\gamma = \mathbf{U^{(1)tr}K^{(1)}U^{(1)}}$ (eigenphase-shift matrix $\pi\mu_\gamma$). δ, τ_1, and τ_2 are specified below in the context of Rydberg vibronic coupling.

Following Ref. [24] we define the reaction matrix $\mathbf{K}^{(2)}$ describing the dissociation process as follows:

$$K^{(2)}_{ii'} = \begin{array}{c} \\ e \\ a \\ d \end{array} \begin{array}{c} \begin{array}{ccc} e & a & d \end{array} \\ \begin{pmatrix} 0 & 0 & \zeta_{ed} \\ 0 & 0 & \zeta_{ad} \\ \zeta_{ed} & \zeta_{ad} & 0 \end{pmatrix} \end{array}. \tag{11}$$

The reaction elements ζ are again real and describe the coupling of the Rydberg channels to the dissociation continuum d. The associated eigenvector matrix is

$$U^{(2)}_{i\alpha} = \begin{array}{c} \\ e \\ a \\ d \end{array} \begin{array}{c} \begin{array}{ccc} \alpha = 1 & 2 & 3 \end{array} \\ \begin{pmatrix} \frac{1}{\sqrt{2}}\cos\beta & \sin\beta & \frac{1}{\sqrt{2}}\cos\beta \\ -\frac{1}{\sqrt{2}}\sin\beta & \cos\beta & -\frac{1}{\sqrt{2}}\sin\beta \\ -\frac{1}{\sqrt{2}} & 0 & \frac{1}{\sqrt{2}} \end{pmatrix} \end{array}, \tag{12}$$

and the diagonalized matrix $\tan\pi\mu_\alpha = \mathbf{U^{(2)tr}K^{(2)}U^{(2)}}$ (eigenphase-shift matrix $\pi\mu_\alpha$) is

$$\begin{pmatrix} -\tan\pi\tau_d & 0 & 0 \\ 0 & 0 & 0 \\ 0 & 0 & +\tan\pi\tau_d \end{pmatrix}, \tag{13}$$

where

$$\tan\beta = -\frac{\zeta_{ad}}{\zeta_{ed}}, \quad \tan\pi\tau_d = \sqrt{\zeta^2_{ed} + \zeta^2_{ad}}. \tag{14}$$

Here β is a channel mixing angle and $\pm\pi\tau_d$ are the eigenphases induced by dissociation. Note that Eq. (8) actually requires the eigenvectors of the matrix $\mathbf{K}^{(2)}_{\gamma\gamma'} = \mathbf{U}^{(2)(tr)}_{\gamma i}\mathbf{K}^{(2)}_{ii'}\mathbf{U}^{(2)}_{i'\gamma'}$ rather than those of $\mathbf{K}^{(2)}_{ii'}$ itself, but this additional transformation does not change the structure of Eq. (11); one merely has to make the substitutions $\zeta_{ed} \to (\zeta_{ed}\cos\delta - \zeta_{ad}\sin\delta)$ and $\zeta_{ad} \to (\zeta_{ed}\sin\delta + \zeta_{ad}\cos\delta)$ in Eqs. (11) and (14), respectively.

E. Elements of the X matrix

The relevant matrix elements of the matrix $\mathbf{X}^{(\text{total})}$ are readily evaluated from Eq. (8), by combining Eqs. (10), (12), and (13), to be

$$\begin{aligned}
X^{(\text{total})}_{ed} &= \sin(2\pi\tau_d)\Big[-\cos(\delta-\beta)\sin\left(\pi\frac{\tau_1-\tau_2}{2}\right) \\
&\quad + i\cos(\delta+\beta)\cos\left(\pi\frac{\tau_1-\tau_2}{2}\right)\Big], \\
X^{(\text{total})}_{ad} &= \sin(2\pi\tau_d)\Big[+\sin(\delta-\beta)\sin\left(\pi\frac{\tau_1-\tau_2}{2}\right) \\
&\quad - i\sin(\delta+\beta)\cos\left(\pi\frac{\tau_1-\tau_2}{2}\right)\Big], \\
X^{(\text{total})}_{ea} &= \sin^2(\pi\tau_d)[\cos 2\delta \sin 2\beta \\
&\quad + \sin 2\delta\cos 2\beta\cos\pi(\tau_1-\tau_2)] \\
&\quad - i\cos^2(\pi\tau_d)[\sin 2\delta\sin\pi(\tau_1-\tau_2)].
\end{aligned} \tag{15}$$

[A phase factor $e^{i\pi(\tau_1+\tau_2)/2}$ common to all elements and irrelevant for the cross sections has been omitted from Eq. (15).] For given matrix elements ζ_{ee}, ζ_{aa}, ζ_{ea}, ζ_{ed}, and ζ_{ad}, the matrices $\mathbf{K}^{(1)}$ and $\mathbf{K}^{(2)}$ may be diagonalized, the eigenphases $\pi\tau_1$, $\pi\tau_2$, and $\pi\tau_d$ as well as the mixing angles

δ and β determined, and hence the elements $\mathbf{X}^{(\mathrm{total})}$ evaluated. These may then be used to evaluate the averaged cross section by means of Eq. (7).

F. Rydberg vibronic coupling

In vibronic frame transformation quantum defect theory [27] for a specific vibrational mode with associated coordinate ρ, the eigenvalues of the reaction matrix $\mathbf{K}$ consist of the continuous infinite set $\tan \pi\mu(\rho)$, where $\mu(\rho)$ is the geometry-dependent fixed-nuclei quantum defect function. The eigenvector matrix consists of the elements $\langle v^+|\rho\rangle \equiv \chi_{v^+}(\rho)$, which are just the set of target vibrational wave functions associated with ρ. In Eq. (8) we may therefore set

$$U_{i\gamma} e^{i\pi\mu_\gamma} = \langle v^+|\rho\rangle e^{i\pi\mu(\rho)}. \tag{16}$$

Instead of using Eq. (16) directly, we remove the continuous eigen-channel set by integrating over ρ [24,26]. We thus consider integrals

$$\xi_{v^+v} = \langle v^+|e^{i\pi\mu(\rho)}|v\rangle, \tag{17}$$

which define a complex unitary matrix of infinite order. The set of vibrational wave functions $\chi_v(\rho)$ may in principle correspond to any potential energy curve [27], but we take it here to coincide with the set of relevant target vibrational wave functions $\chi_{v^+}(\rho)$. The notation v instead of v^+ is used merely for formal distinction of the asymptotic channels i and the channels γ. In our specific problem (cf. Fig. 2) we retain only the two vibronic channels $e = v^+ = 0$ and $a = v^+ = 1$, and correspondingly we use $v = 0$ and $v = 1$.

While the matrix defined by the elements of Eq. (17) is unitary and could serve as the Jost matrix $\mathbf{J}^{(1)}_{i\gamma}$, Eq. (10), the unitarity is actually lost when only two functions of the infinite vibrational basis are retained, as is done here. We therefore set up the reaction matrix $\mathbf{K}^{(1)}$ directly in terms of the elements $\zeta_{v^+v} = \langle v^+|\tan\pi\mu(\rho)|v\rangle$ [closely related to Eq. (17), with v^+, v taking the values 0 and 1], diagonalize it, and thus obtain the phase angle δ and the eigenphases $\pi\tau_1$ and $\pi\tau_2$. The unitarity of $\mathbf{J}^{(1)}$ is preserved by this procedure. This is done in Sec. II G.

G. Linear harmonic approximation

The $v^+ = 0$ and 1 vibrational wave functions are usually well approximated by those of the harmonic oscillator. (Highly floppy systems are exceptions which we do not consider here.) At the same time the quantum defect $\mu(\rho)$ may be expanded for small vibrational amplitudes according to $\mu(\rho) \sim \mu(\rho = \rho_e) + \frac{\partial\mu}{\partial\rho}|_{\rho=\rho_e}(\rho - \rho_e)$, where ρ_e is the equilibrium value of the coordinate ρ. Expanding in addition the tan function linearly around ρ_e, we have [cf. Eq. (9)]

$$\begin{aligned} \zeta_{ee} &= \zeta_{aa} \sim \tan\pi\mu(\rho_e), \\ \zeta_{ea} &= \zeta_{ae} \sim \pi \left.\frac{\partial\mu}{\partial\rho}\right|_{\rho=\rho_e} \langle v^+ = 0|\rho - \rho_e|v = 1\rangle. \end{aligned} \tag{18}$$

Here well-known analytic expressions for a one- or two-dimensional oscillator may be substituted for the vibrational integral appearing in the second line of Eq. (18). With Eq. (18) the eigenvalues of $\mathbf{K}^{(1)}$ become $\tan\pi\tau_{1\text{ or }2} = \zeta_{ee} \pm \zeta_{ea}$ and we have $\delta = \pi/4$. In the following we remove the common diagonal elements $\zeta_{ee} = \zeta_{aa}$ from the matrix $\mathbf{K}^{(1)}$ as they do not contribute to the scattering matrix element S_{ed} which we determine here.

III. LIMITING CASES

A. Dominating indirect coupling, no direct coupling: $\zeta_{ed} = 0$

We first examine the situation of vanishing direct coupling, which was assumed in Refs. [5–7], and we use the linear harmonic approximation. This situation may be applicable when no potential surface crossing with a dissociative state occurs near the equilibrium geometry of the recombining ion, and therefore $\zeta_{ed} \approx 0$. ζ_{ad}, on the other hand, may differ from zero because the vibrationally excited wave function extends farther in configuration space so that Franck-Condon factors are more favorable, or else because vibronic coupling effects are stronger when the vibrational excitation increases. When $\zeta_{ed} = 0$, Eqs. (14) yield $\beta = \pi/4$ and $\tan\pi\tau_d = \zeta_{ad}$. Equations (15) then give

$$\begin{aligned} X^{(\mathrm{total})}_{ed} &= -\frac{\zeta_{ea}}{\sqrt{1+\zeta^2_{ea}}} \frac{2\zeta_{ad}}{(1+\zeta^2_{ad})}, \\ X^{(\mathrm{total})}_{ad} &= -i\frac{1}{\sqrt{1+\zeta^2_{ea}}} \frac{2\zeta_{ad}}{(1+\zeta^2_{ad})}, \\ X^{(\mathrm{total})}_{ea} &= -i\frac{2\zeta_{ea}}{(1+\zeta^2_{ea})} \frac{1}{(1+\zeta^2_{ad})}. \end{aligned} \tag{19}$$

Substituting $\zeta_{ij} \to \tan(\pi\mu_{ij})$ we obtain from Eq. (7)

$$\begin{aligned} \langle\sigma\rangle &= \frac{4\pi r}{k^2}\sin^2(\pi\mu_{ea})\left[\frac{\sin^2(\pi\mu_{ad})\cos^2(\pi\mu_{ad})}{1-\cos^2(\pi\mu_{ea})\cos^2(\pi\mu_{ad})}\right] \\ &\equiv \frac{4\pi r}{k^2}\sin^2(\pi\mu_{ea})F^{(ea)}, \quad \epsilon = \frac{1}{2}k^2 \leqslant E^+_a, \\ \sigma &= \frac{4\pi r}{k^2}\sin^2(\pi\mu_{ea})[\sin^2(\pi\mu_{ad})\cos^2(\pi\mu_{ad})] \\ &\equiv \frac{4\pi r}{k^2}\sin^2(\pi\mu_{ea})G^{(ea)}, \quad \epsilon = \frac{1}{2}k^2 > E^+_a. \end{aligned} \tag{20}$$

The two Eqs. (20) may be compared with the averaged Breit-Wigner expression, Eq. (1). The factors $F^{(ea)}$ and $G^{(ea)}$, defined by the second identity of each expression, play the role of correction factors to the corresponding Breit-Wigner result, Eqs. (1), which for $\sin(\pi\mu_{ea}) \approx \pi\mu_{ea}$ correspond to $F^{(ea)} = 1$ and $G^{(ea)} = 0$. These correction factors account for the reionization processes occurring after capture, neglected in the Breit-Wigner theory.

The quantity $\sigma/\langle\sigma\rangle = G/F$ tells us by which factor the cross section is reduced when the energy passes through the threshold E^+_a. We define the relative *height* of the *downward step* which occurs at the threshold E^+_a of the active Rydberg channel as

$$H = 1 - \frac{\sigma}{\langle\sigma\rangle} = 1 - \frac{G^{(ea)}}{F^{(ea)}} = \cos^2(\pi\mu_{ea})\cos^2(\pi\mu_{ad}). \tag{21}$$

The Breit-Wigner theory predicts the cross section will drop to zero at E^+_a, that is, $H = 1$ in this case.

Figure 3 [left-hand panels (a) and (c)] displays the factors $F^{(ea)}$, $G^{(ea)}$, and H obtained with the three-channel model for $\zeta_{ed} \equiv \tan(\pi\mu_{ed}) = 0$ [Eqs. (20) and (21)], plotted as functions of the coupling to dissociation, μ_{ad}, for various values of

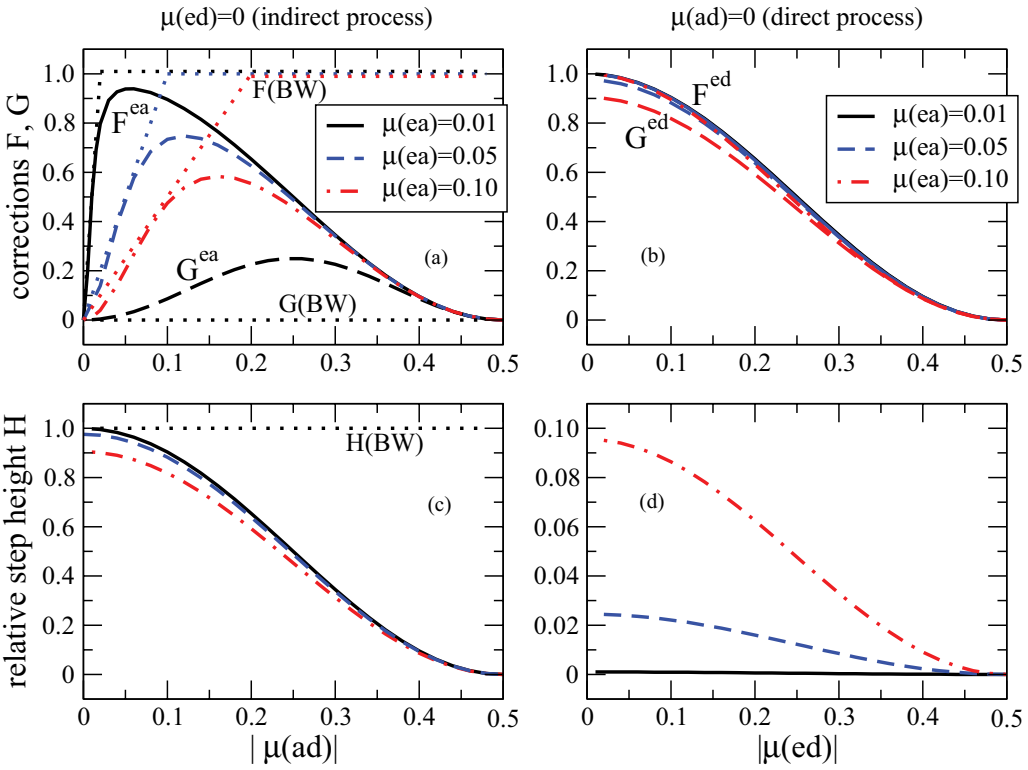

FIG. 3. (Color online) Top panels (a) and (b): Correction factors F and G. Bottom panels (c) and (d): Relative height H of the downward step at the $v^+ = 1$ threshold. F and H are plotted as functions of the coupling strength to the dissociation continuum, for various values of the capture strength μ_{ea}: $\mu_{ea} = 0.01$ full black line, 0.05 dashed line (blue online), and 0.10 dot-dashed line (red online). The factors G are indicated by long-dashed lines. Left panels (a) and (c): pure indirect process. The Breit-Wigner values $F(BW)$, $G(BW)$, and $H(BW)$ are indicated by dotted lines (in the appropriate colors online) in panels (a) and (c). Right panels (b) and (d): pure direct process. Note the difference of the scales of panels (c) and (d). See the text for further details.

the capture quantum defect, μ_{ea}. For comparison the figure also shows the values obtained in the framework of the Breit-Wigner theory, including refinements of Eq. (1) derived in Ref. [7] for values of $|\mu_{ad}|$ comparable or smaller than $|\mu_{ea}|$. We discuss this situation first. When $|\mu_{ad}| \ll |\mu_{ea}|$, dissociation is so weak that the captured electron reionizes before having a chance to pass into the dissociation channel. $F^{(ea)}$ therefore tends to zero in this limit, as is also predicted by the refined Breit-Wigner model. When $|\mu_{ad}| \approx |\mu_{ea}|$ one has $F^{(ea)} \approx 0.5$, an interesting result, again obtained both in three-channel model and the Breit-Wigner formalism [7]. Turning now to situations where $|\mu_{ad}| \geqslant |\mu_{ea}|$, we see from Fig. 3 that the Breit-Wigner theory is reliable when the vibronic coupling term $|\mu_{ea}|$ is quite small and $|\mu_{ad}|$ is also rather small. The assumption $|\mu_{ad}| \gg |\mu_{ea}|$ underlying Eq. (1) turns out to be not very stringent: Indeed, we see that $|\mu_{ad}| \approx 2$ to $5 \times |\mu_{\rm ea}|$ (the best value depends on μ_{ea}) yields the best agreement with the BW expression. By contrast, when the coupling $|\mu_{ad}|$ gets very strong, counterintuitive nonlinear multichannel effects quickly take over, enhancing reionization and causing the correction factor $F^{(ea)}$ to fall progressively further below unity. At the same time $G^{(ea)}$ (which would be zero according to the BW theory) increases, thereby rapidly diminishing the step height H.

These findings do not severely limit the applicability of Eq. (1), because vibronic coupling in molecules tends to be intrinsically rather weak so that in effect real systems always correspond to situations close to the abscissas in Fig. 3. The Jahn-Teller effect in H_3 with $\mu_{ea} = 0.052$ [6] [corresponding very nearly to the dashed curves (blue online) in Figs. 3(a) and 3(c)] is indeed an example of an exceptionally strong vibronic effect. The practical use of Fig. 3 is illustrated in Sec. V A below with the example of H_3^+ recombination.

B. Dominating direct coupling, no indirect coupling: $\zeta_{ad} = 0$

This situation is the exact opposite of that discussed in Sec. III A: An electronic surface crossing with a dissociative state occurs near the equilibrium geometry of the ion in such a way that the Franck-Condon factors yield a much larger value for ζ_{ed} than for ζ_{ad}. In this case, where the direct coupling dominates and the active Rydberg series is not coupled to the dissociation continuum, Eqs. (14) yield $\beta = -\pi/4$ and $\tan \pi\tau_d = \zeta_{ed}$. Equations (15) then give

$$
\begin{aligned}
X_{ed}^{(\rm total)} &= i\,\frac{1}{\sqrt{1+\zeta_{ea}^2}}\,\frac{2\zeta_{ed}}{(1+\zeta_{ed}^2)},\\
X_{ad}^{(\rm total)} &= \frac{\zeta_{ea}}{\sqrt{1+\zeta_{ea}^2}}\,\frac{2\zeta_{ed}}{(1+\zeta_{ed}^2)},\\
X_{ea}^{(\rm total)} &= -i\,\frac{2\zeta_{ea}}{(1+\zeta_{ea}^2)}\,\frac{1}{(1+\zeta_{ed}^2)}.
\end{aligned}
\tag{22}
$$

The analog of Eqs. (20) now becomes

$$\begin{aligned}\langle\sigma\rangle &= \frac{4\pi r}{k^2}\sin^2(\pi\mu_{ed})\left[\frac{\cos^2(\pi\mu_{ea})\cos^2(\pi\mu_{ed})}{1-\sin^2(\pi\mu_{ea})\cos^2(\pi\mu_{ed})}\right]\\ &\equiv \frac{4\pi r}{k^2}\sin^2(\pi\mu_{ed})F^{(ed)}, \quad \epsilon = \frac{1}{2}k^2 \leqslant E_a^+,\\ \sigma &= \frac{4\pi r}{k^2}\sin^2(\pi\mu_{ed})\left[\cos^2(\pi\mu_{ea})\cos^2(\pi\mu_{ed})\right]\\ &\equiv \frac{4\pi r}{k^2}\sin^2(\pi\mu_{ea})G^{(ed)}, \quad \epsilon = \frac{1}{2}k^2 > E_a^+, \end{aligned} \tag{23}$$

and the relative step height is given by

$$H = 1 - \frac{\sigma}{\langle\sigma\rangle} = 1 - \frac{G^{(ed)}}{F^{(ed)}} = \sin^2(\pi\mu_{ea})\cos^2(\pi\mu_{ed}). \tag{24}$$

The factors $F^{(ed)}$, $G^{(ed)}$, and H for the case of a dominant direct coupling of the entrance channel to the dissociation continuum are plotted in the right-hand panels (b) and (d) of Fig. 3 as functions of the coupling to dissociation, μ_{ed}, for various values of the capture quantum defect, μ_{ea}. We see, not surprisingly, that capture processes into the Rydberg channel have little influence in this situation, even though a small downward step may also occur when $|\mu_{ea}|$ is large [dot-dashed curve (red online) in Fig. 3(d)]. Again, as we have seen for the case of indirect processes [panels (a) and (c) of Fig. 3], real situations correspond to rather small values of the effective interactions, typically well below ≈0.2. For instance the electronic coupling μ_{ed} dominating the DR of the NO^+ ion—one of the classic examples of a strong Rydberg-valence direct interaction which yields no step feature at all—is known to amount to $\mu_{ed} = 0.063$ only [28], a value situated close to the abscissa in the panels (b) and (d) of Fig. 3, where $F^{(ed)}$ and $G^{(ed)}$ are close to unity.

IV. INTERMEDIATE SITUATIONS

The expressions (15) together with the linear harmonic approximation, Eq. (18), can be used to evaluate averaged DR cross sections by means of Eq. (7) for intermediate situations where both the direct and indirect processes are present, that is, $\zeta_{ed} \neq 0$ and simultaneously $\zeta_{ad} \neq 0$. In an intermediate situation we may compare the calculated cross section both with the limiting expression $(4\pi r/k^2)\sin^2(\pi\mu_{ea})$ as well as with $(4\pi r/k^2)\sin^2(\pi\mu_{ed})$, and hence alternatively define correction factors $F^{(ea)}$ and $F^{(ed)}$ (and, of course, the corresponding quantities $G^{(ea)}$ and $G^{(ed)}$). Large deviations of $F^{(ea)}$ or $F^{(ed)}$ from unity then tell us whether the direct or indirect process tend to dominate. The relative step height is always given by $H = 1 - \sigma/\langle\sigma\rangle$, that is, in terms of the ratio of the continuum cross section above the $v^+ = 1$ threshold divided by the resonance-averaged cross section below.

Figure 4 is a chart intended to allow the assessment of the relative importance of the indirect and direct DR processes, respectively, based on observed relative step heights and cross-sectional values. The figure presents an array of plots of the correction factors $F^{(ea)}$, $F^{(ed)}$, and relative step heights H, as functions of the coupling strength μ_{ed}, for various assumed values of the Rydberg capture coupling, μ_{ea}, and Rydberg dissociative coupling, μ_{ad}. Each plot corresponds for $\mu_{ed} = 0$

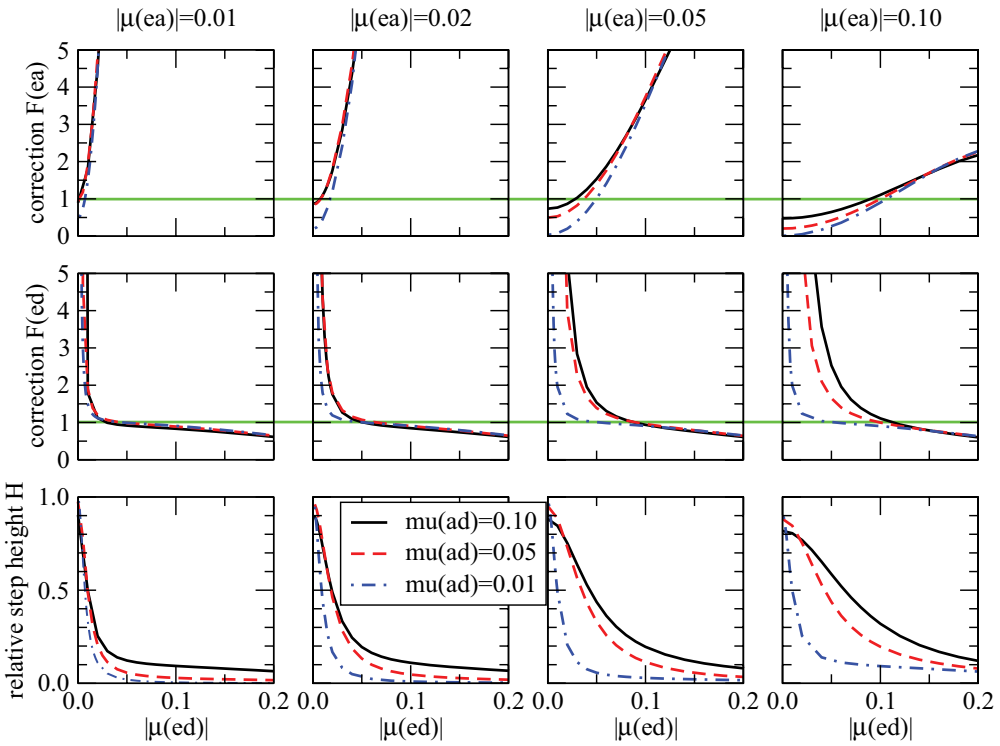

FIG. 4. (Color online) Correction factors F and relative step heights H in intermediate situations ($\mu_{ad} \neq 0$, $\mu_{ed} \neq 0$) as functions of the direct coupling strength μ_{ed}. Top row of panels: correction factors $F^{(ea)}$ for various values of μ_{ea} and μ_{ad}, as indicated. Second row of panels: corresponding correction factors $F^{(ed)}$. Bottom row of panels: relative step heights H. See the text for details.

to the situation discussed in Sec. III A above and approaches for increasing values the situation discussed in Sec. III B.

The array of plots as a whole indicates in a quantitative manner how the direct process takes over as μ_{ed} increases. Basically, we see that for small values of μ_{ed} the correction factor $F^{(ea)}$ is near unity or not too far from it, whereas for increasing μ_{ed} typically we find $F^{(ea)} \gg 1$. The correction factor $F^{(ed)}$ behaves in the opposite way: For small values of μ_{ed} it is $\gg 1$, whereas it approaches values not too far from unity for larger μ_{ed}. We further see that as the Rydberg capture coupling μ_{ea} becomes larger, the indirect process resists the competition of the increasing direct process longer. At the same time the remarks made in Sec. III A concerning the relative magnitudes of μ_{ea} and μ_{ad} remain valid: μ_{ad} must be larger than μ_{ea} for the indirect process to remain significant. The horizontal lines (green online) in the top and second rows of panels in Fig. 4 indicate the values $F = 1$. Whenever the curves $F^{(ea)}$ or $F^{(ed)}$ approach these lines, this means that the predicted resonance-averaged cross section $\langle\sigma\rangle$ is near the value $(4\pi r/k^2)\sin^2(\pi\mu_{ea})$ and/or $(4\pi r/k^2)\sin^2(\pi\mu_{ed})$. The use of Fig. 4 is illustrated in Sec. V B below with the example of HCO^+ dissociative recombination.

V. DISCUSSION

A. Dissociative recombination of H_3^+

It is instructive to re-examine the DR of H_3^+ to which the Breit-Wigner expression, Eq. (1), has been applied previously [6]. H_3^+ is a good example of a pure indirect process implying $\zeta_{ed} \approx 0$, as we know since the important work of Kokoouline *et al.* [29]. The recent experimental data of Kreckel *et al.* taken at the ion storage ring Test Storage Ring (TSR) [14] indicate that the DR cross section falls very nearly by one order of magnitude at the $v_2^+ = 1$ threshold of H_3^+. This is borne out in their Fig. 7 (see also the present Fig. 1), which also shows that their data are consistent with the earlier CRYRING data from Ref. [15]. In terms of our present definitions this means that the observed relative step height amounts to $H \approx 0.9$. Within the framework of the present three-channel model the value $\mu_{ea} = 0.05$ used in Ref. [6] implies, together with this value for H, that $\mu_{ad} \approx 0.10$, a value just twice as large as μ_{ea}. This may be inferred by inspection from Fig. 3(c) (dashed curve, blue online). Further, the dashed curve (blue online) in Fig. 3(a) indicates that for this case we have $F \approx 0.75$. This in turn means that the cross section below the threshold predicted by the three-channel model would be $\approx$25% lower than the value predicted by Eq. (1).

We may summarize the situation by saying that based on the present three-channel model and the observed relative step size at 0.313 eV, we find that (i) we can get an estimate of the value μ_{ad} of the coupling of the active Rydberg series to the dissociation continuum, and on the other hand, (ii), for electron energies lower than 0.313 eV the three-channel model predicts a cross section lower by about 25% than what was predicted in Ref. [6]. Such a reduction appears as a rather minor effect on a logarithmic plot such as generally used for the representation of DR measurements spanning several orders of magnitude. We nevertheless note that a very recent re-evaluation of the Jahn-Teller effect in H_3 [13] indicates that the value μ_{ea} was underestimated in Ref. [6] and that their cross section values should be increased by about 15%. This partially compensates for the reduction due to inclusion of reionization in the three-channel model. We thus conclude that the three-channel model appears to be consistent with experimental DR measurements and with the value for μ_{ea} deduced from H_3 bound-state spectroscopy [6], if we assume a value $\mu_{ad} \approx 0.1$. Figure 1 (dashed curves, blue online) shows that the rate coefficient as a function of the energy evaluated by means of Eq. (20) (with the updated value of μ_{ea} [13] and the value of μ_{ad} determined here) indeed fits the observed step height reasonably well. The second step near $v_2^+ = 2$, however, is not reproduced by the three-channel treatment as it involves $\Delta v_2^+ = 2$ interactions, which we ignore here. We stress once again that the coupling μ_{ad} estimated here is an effective quantity, which in fact is likely be the result of multistep interactions between the active channel a and the dissociation channel d, via a chain of intermediate Rydberg channels $a', a'', \ldots$ involving increasing vibrational excitation.

B. Dissociative recombination of HCO^+

The Breit-Wigner expression Eq. (1) was applied to the dissociative recombination of HCO^+ a few years ago, assuming that the mechanism driving the process is the $p\pi \sim s\sigma$ interaction induced by Renner-Teller coupling when the target ion bends [4,5]. However, the recombination rates predicted in this way were by about a factor 2 to 6 below the observed rates of Refs. [30,31]. At the same time only a very small step, if any, is apparent at the $v_2^+ = 1$ threshold of HCO^+ at $\epsilon = 0.103$ eV, as shown in particular by Fig. 4 of Ref. [32]. This raises the question of whether a direct process might also contribute. HCO^+ is isoelectronic with NO^+, and similar electronic Rydberg-valence interactions like in NO must also exist in HCO, while the Renner-Teller interaction, a strong vibronic nonadiabatic effect, is of course absent in diatomic NO. The corresponding surface crossings may be less favorable in HCO than in NO for the occurrence of a significant direct DR process. Indeed, Larson *et al.* [33], in their *ab initio* calculations, did not find a favorable crossing between the HCO^+ ground state and the dissociative $^2A'$ state of HCO. On the other hand, the absence of a surface crossing does not necessarily mean that there is no direct DR process, as is known from the example of CH^+ [34]. New theoretical calculations by Larson *et al.* [32] take account of direct as well as indirect (Renner-Teller) processes in HCO but do not cover the low energy range $\leqslant$0.103 eV that we are interested in here.

These discrepancies prompt us to use our present parametric three-channel approach in order to estimate what coupling strength μ_{ed} would be required to bring experiment and theory into agreement at low energies. The Rydberg capture coupling has been evaluated in Ref. [5] from Rydberg spectroscopic data to be about $\mu_{ea} = 0.02$. (Actually, two capture processes, mediated by Renner-Teller $s\sigma \rightarrow p\pi$ as well as $p\pi \rightarrow s\sigma$ coupling, were considered in Ref. [5], which have somewhat different values, but for simplicity we use here their average.) Further, as already stated, the thus predicted low-energy DR cross section is on the average too low by a factor $\approx$4. Inspection of the curves $F^{(ea)}$ in Fig. 4 for $\mu_{ea} = 0.02$ indicates that the necessary correction $F^{(ea)} \approx 4$ is reached for

$\mu_{ed} \approx 0.04$, almost independently of the value of μ_{ad}. Careful inspection of the experimental cross sections reproduced in Fig. 4 of Ref. [32] further suggests that the small step barely visible near the $v_2^+ = 1$ threshold corresponds, very approximately, to $H \approx 0.2$. We next examine the predicted relative step heights for $\mu_{ea} = 0.02$ in the lowest row of the plot array of Fig. 4. There it is seen that $H \approx 0.2$ is compatible with $\mu_{ad} \approx 0.05$. Therefore we conclude that the set of values $\mu_{ea} = 0.02$, $\mu_{ed} = 0.04$, $\mu_{ad} = 0.05$ is roughly compatible with the observations. We stress again, as in the preceding discussion of H_3^+ DR, that the values for μ_{ad} and μ_{ed} estimated here are effective quantities which possibly are not related in a simple way to corresponding quantities calculated from first principles.

C. Autoionization and predissociation widths of Rydberg states

The channel interaction parameters estimated in Secs. V A and V B for H_3 and HCO imply autoionization and predissociation widths of the molecular Rydberg states of the active series involved in the process. These could in principle be calculated from the scattering matrix Eq. (6), but we may equivalently use the Rydberg Fermi Golden rule expression [10]

$$\Gamma_j = 2\pi \frac{2\mathcal{R}}{n_a^{*3}} \mu_{aj}^2. \tag{25}$$

Here, Γ_j ($j = e$ or d) is the partial autoionization width ($j = e$) or predissociation width ($j = d$), respectively, while μ_{aj} is the quantum defect matrix element coupling the Rydberg channel a to the continuum e or d (cf. Fig. 2). $\mathcal{R}$ is the Rydberg constant as before, and n_a^* is the effective principal quantum number of the individual member of the active Rydberg series considered. The total width is then $\Gamma = \Gamma_e + \Gamma_d$. For our estimates we assume that the autoionized and predissociated Rydberg level is not mixed, that is, that it corresponds purely to $v_2^+ = 1$ or 0. Further, we ignore rotational motion which (via the appropriate frame transformation) also affects the resonance widths. Table I lists a few partial and total level widths estimated by means of Eq. (25) and compares them with values estimated on the basis of optical-optical double-resonance Rydberg spectra published by Helm and collaborators for H_3 [35,36] and by Grant and collaborators for HCO [37]. These experimental values are not much more than visual estimates based on the broadest features seen in the region above the relevant v_2^+ thresholds E_e^+. The values for HCO $v_2^+ = 0$ listed in Table I correspond to the range $E < E_a^+$ in Fig. 2, where the channel e is closed and may be predissociated via the coupling μ_{ed}.

TABLE I. Autoionization and predissociation widths of Rydberg levels (cm^{-1}).

		μ_{ea}	μ_{ad}	μ_{ed}	n_a^*	Γ_e	Γ_d	$\Gamma_e + \Gamma_d$	Γ(expt.)
H_3	$v_2^+ = 1$	0.05	0.10		8	7	27	34	3[a]
					20	0.4	1.7	2.1	1[b]
HCO	$v_2^+ = 1$	0.02	0.05		13	0.3	1.6	1.9	0.8[c]
	$v_2^+ = 0$			0.04	13	0	1.0	1.0	

[a]Rough estimate based on the spectra plotted in Figs. 7 and 9 of Refs. [35] and [36].

[b]Rough estimate based on the spectra plotted in Figs. 7(e) and 7(f) of Ref. [40].

[c]Rough estimate based on the spectrum plotted in Fig. 4 of Ref. [37].

Table I shows that the observed widths of H_3 and HCO are smaller than those implied by the dissociative recombination data. For HCO the discrepancy corresponds to a factor of 2 and may be attributed to the rough nature of our estimates. For H_3 the discrepancy is as large as an order of magnitude. This disagreement may appear surprising at first sight, but it should be realized that the strongly predissociated Rydberg states which drive the DR process are not likely to appear prominently in the resonantly enhanced multiphoton photoionization spectra because the population is diverted into the dissociation channel. In other words, the structures seen in those spectra are probably for a good part *just not* the ones active in DR. This well-known effect has been documented in detail experimentally [38] and theoretically [39] in the manifold of triplet gerade Rydberg states of H_2. Helm and collaborators [40] have carried out an experiment on H_3 where they monitored both the ionization and dissociation fragment channels. This work concerned mostly the s Rydberg channels, which are not so important for DR, but their Figs. 7(e) and 7(f) show the example of a $20pe'$ resonance which is indeed quite broad and seen most prominently in the dissociation channel. The discrepancy between the three-channel formula and the observation is reduced to a factor of 2 in this case (cf. Table I).

VI. CONCLUSIONS

The three-channel DR model developed here represents an extension of the two-channel Breit-Wigner model of Ref. [6] applicable to indirect dissociative recombination at low electron energies ($\epsilon \leqslant 0.2$ eV). The present refinement takes account of the following processes which were omitted in Ref. [6]: (i) Reionization (or autoionization) of the collision complex which may occur after electron capture into vibrationally excited Rydberg states and which competes with predissociation leading to DR, and (ii) competition between direct and indirect DR processes.

Figure 3 of the present paper should be helpful for the assessment of the accuracy and reliability of the simple Breit-Wigner approach. It has allowed us here to confirm the validity—to within about 25%—of the earlier application to H_3 [6]. Figure 4 is designed to help experimentalists interpret their results and determine the relative importance of the direct and indirect processes based on the observed Rydberg resonance-averaged cross section at low energy and the relative step height H observed near the first vibrational threshold. We have used it here in order to make a guess at the relative contributions of the direct and indirect processes in HCO. Some knowledge of the vibronic coupling parameter (quantum defect) μ_{ea} connecting the entrance and the active electron-ion Rydberg channels is always necessary, but it turns out that this quantity may be characterized by means of Rydberg spectroscopy (H_3^+, HCO^+ [5,6]) or by first principles calculations (HCO^+, H_3O^+, NH_4^+ [4,41,42]), probably more easily than the elusive interactions with the dissociation channels.

By combining experimental DR data with the use of Figs. 3 and 4 we have been able to extract approximate values for the dissociative couplings μ_{ad} and μ_{ed} in H_3 and HCO. We have tested these by estimating autoionization and predissociation widths of some highly excited individual Rydberg states in the relevant spectral regions of H_3^+ and HCO. The resonances observed in the published experimental REMPI experiments are considerably narrower than these estimates, and we attribute this discrepancy to the fact that the strongly predissociated Rydberg states which are involved in the DR process are not likely to be observed in multiphoton ionization experiments. Beyond the efforts made in Ref. [40], it would seem worthwhile to test this hypothesis by systematic double-resonance experiments where the dissociation channels are monitored and where these resonances should appear.

It should not be overlooked, of course, that the present model is set up in terms of a minimal set of effective channels. We have completely ignored the rotational structure. Further, in real molecules, multichannel effects may play an important role, such as shown for the dissociative recombination of LiH^+ by Čurík and Greene [43]. Complex resonances [44] possessing a rich fine structure may be formed, which permit the exchange of several quanta of vibrational energy between a slow free electron and an ion core, rather than just a single one as envisioned here. Part of these phenomena are effectively included in our simplified model as discussed in Sec. II A. However, for instance, the appearance of a second step near $v_2^+ = 2$ in the experimental spectra of Fig. 1 is a sign of the occurrence of multichannel effects not taken into account here, as is the irregularity of the resonance structure seen at lower energies.

Finally, we stress that the present approach aims at providing experimentalists studying dissociative recombination with a tool that allows them to discuss their data in qualitative or semiquantitative terms and extract information on the interactions at play without having to resort to sophisticated large-scale calculations. We hope that this spectroscopy of dissociative recombination will prove useful in the future.

ACKNOWLEDGMENTS

This work has greatly benefited from our extensive discussions with Dr. S. T. Pratt (Argonne). We thank him for his careful reading of the manuscript and for his numerous helpful suggestions. We thank Dr. H. Kreckel, B. McCall (Urbana, Illinois) and Dr. O. Novotný (New York) for communicating their original experimental cross-sectional data for H_3^+ taken at the TSR and CRYRING storage rings as well as for helpful correspondence. I.F.S. and Ch.J. thank the ANR (France) for financial support under Contract No. 09-BLAN-020901 and the International Atomic Energy Agency (Vienna, Austria) for CRP contracts. Ch.J. also received partial support from the Ernst Miescher Foundation (Basel, Switzerland). I.F.S. further acknowledges the scientific and financial support from the European Space Agency, the French network Fédération de Recherche Fusion Magnétique Controlée, the CNRS/INSU (France, program Physique et Chimie du Milieu Interstellaire), and the Région Haute Normandie (France, CPER contract). I.F.S. finally thanks the Laboratoire Aimé Cotton for hospitality during his frequent visits and Dr. F. Lique (Le Havre) for discussions. N.P. has been supported in part by the strategic grant POSDRU/21/1.5/G/13798, in the framework of the POSDRU Romania 2007-2013, cofinanced by the European Social Fund "Investing in People."

[1] D. R. Bates, Phys. Rev. **78**, 492 (1950).
[2] J. N. Bardsley, J. Phys. B **1**, 365 (1968).
[3] J. C. Y. Chen and M. H. Mittleman, in *Abstracts of the Fifth International Conference on Atomic Collisions* (Leningrad, Nauka, 1967), p. 329.
[4] I. A. Mikhaylov, V. Kokoouline, Å. Larson, S. Tonzani, and C. H. Greene, Phys. Rev. A **74**, 032707 (2006).
[5] Ch. Jungen and S. T. Pratt, J. Chem. Phys. **129**, 164311 (2008).
[6] Ch. Jungen and S. T. Pratt, Phys. Rev. Lett. **102**, 023201 (2009).
[7] Ch. Jungen and S. T. Pratt, J. Chem. Phys. **133**, 214303 (2010).
[8] S. T. Pratt and Ch. Jungen, J. Phys.: Conf. Ser. **300**, 012019 (2011).
[9] R. S. Berry, J. Chem. Phys. **45**, 1228 (1966).
[10] G. Herzberg and Ch. Jungen, J. Mol. Spectrosc. **41**, 425 (1972).
[11] P. M. Dehmer and W. A. Chupka, J. Chem. Phys. **65**, 2243 (1976).
[12] S. T. Pratt, Annu. Rev. Phys. Chem. **56**, 281 (2005).
[13] Ch. Jungen, M. Jungen, and S. T. Pratt, Philos. Trans. R. Soc. A **370**, 5074 (2012).
[14] H. Kreckel, O. Novotný, K. N. Crabtree *et al.*, Phys. Rev. A **82**, 042715 (2010).
[15] B. J. McCall, A. J. Huneycutt, R. J. Saykally *et al.*, Nature (London) **422**, 500 (2003).
[16] S. F. dos Santos, V. Kokoouline, and C. H. Greene, J. Chem. Phys. **127**, 124309 (2007).
[17] A. Petrignani, S. Altevogt, M. H. Berg *et al.*, Phys. Rev. A **83**, 032711 (2011).
[18] A. Tramer, Ch. Jungen, and F. Lahmani, *Energy Dissipation in Molecular Systems* (Springer, Berlin, 2005).
[19] M. J. Seaton, Rep. Prog. Phys. **46**, 167 (1983) (reprinted in Ref. [20]).
[20] Ch. Jungen, ed., *Molecular Applications of Quantum Defect Theory* (Institute of Physics, Bristol, 1996).
[21] M. Gailitis, Sov. Phys. JETP **17**, 1328 (1963) (reprinted in Ref. [20]).
[22] Ch. Jungen and S. C. Ross, Phys. Rev. A **55**, R2503 (1997).
[23] A. Matzkin, Ch. Jungen, and S. C. Ross, Phys. Rev. A **62**, 062511 (2000).
[24] A. Giusti, J. Phys. B **13**, 3867 (1980) (reprinted in Ref. [20]).
[25] F. O. Waffeu Tamo, H. Buhr, O. Motapon *et al.*, Phys. Rev. A **84**, 022710 (2011).
[26] C. H. Greene and Ch. Jungen, Adv. At. Mol. Phys. **21**, 51 (1985).

[27] Ch. Jungen and O. Atabek, J. Chem. Phys. **66**, 5584 (1977) (reprinted in Ref. [20]).
[28] M. Raoult, J. Chem. Phys. **87**, 4736 (1987).
[29] V. Kokoouline, C. H. Greene, and B. D. Esry, Nature (London) **412**, 891 (2001).
[30] A. Le Padellec, C. Sheehan, D. Talbi, and J. B. A. Mitchell, J. Phys. B **30**, 319 (1997).
[31] C. Sheehan, Ph.D. thesis, University of Western Ontario, 2000 (unpublished).
[32] Å. Larson, M. Stenrup, and A. E. Orel, Phys. Rev. A **85**, 042702 (2012).
[33] Å. Larson, S. Tonzani, R. Santra, and C. H. Greene, J. Phys.: Conf. Ser. **4**, 148 (2005).
[34] L. Carata, A. E. Orel, M. Raoult, I. F. Schneider, and A. Suzor-Weiner, Phys. Rev. A **62**, 052711 (2000).
[35] M. C. Bordas, L. J. Lembo, and H. Helm, Phys. Rev. A **44**, 1817 (1991).
[36] I. Mistrík, R. Reichle, U. Müller, H. Helm, M. Jungen, and J. A. Stephens, Phys. Rev. A **61**, 033410 (2000).
[37] E. Mayer and E. R. Grant, J. Chem. Phys. **103**, 10513 (1995).
[38] L. J. Lembo, N. Bjerre, D. L. Huestis, and H. Helm, J. Chem. Phys. **92**, 2219 (1990).
[39] A. Matzkin, Ch. Jungen, and S. C. Ross, Phys. Rev. A **62**, 062511 (2000).
[40] I. Mistrík, R. Reichle, H. Helm, and U. Müller, Phys. Rev. A **63**, 042711 (2001).
[41] N. Douguet, A. E. Orel, C. H. Greene, and V. Kokoouline, Phys. Rev. Lett. **108**, 023202 (2012).
[42] N. Douguet, V. Kokoouline, and A. E. Orel, J. Phys. B **45**, 051001 (2012).
[43] R. Čurík and C. H. Greene, Mol. Phys. **105**, 1565 (2007).
[44] Ch. Jungen and M. Raoult, Faraday Discuss. Chem. Soc. **71**, 253 (1981).